Application of Biomagnetic Fluid Dynamics modeling for simulation of flow with magnetic particles and variable fluid properties over a stretching cylinder

Article *in* Mathematics and Computers in Simulation · April 2022

DOI: 10.1016/j.matcom.2022.04.008

CITATIONS
27

READS
430

4 authors:

Md. Ghulam Murtaza Talukder
Comilla University
69 PUBLICATIONS **365** CITATIONS
SEE PROFILE

Md. Jahangir Alam
Comilla University
29 PUBLICATIONS **156** CITATIONS
SEE PROFILE

Mohammad Ferdows
University of Dhaka
226 PUBLICATIONS **3,520** CITATIONS
SEE PROFILE

Efstratios Tzirtzilakis
University of Peloponnese
96 PUBLICATIONS **1,922** CITATIONS
SEE PROFILE

Available online at www.sciencedirect.com
ScienceDirect
Mathematics and Computers in Simulation 199 (2022) 438–462
MATHEMATICS AND COMPUTERS IN SIMULATION
www.elsevier.com/locate/matcom

Original articles

Application of Biomagnetic Fluid Dynamics modeling for simulation of flow with magnetic particles and variable fluid properties over a stretching cylinder

Jahangir Alam[a], M.G. Murtaza[b], E.E. Tzirtzilakis[c,*], M. Ferdows[a]

[a] *Research Group of Fluid Flow Modeling and Simulation, Department of Applied Mathematics, University of Dhaka, Dhaka 1000, Bangladesh*
[b] *Department of Mathematics, Comilla University, Cumilla 3506, Bangladesh*
[c] *Fluid Mechanics and Turbomachinary Laboratory, Department of Mechanical Engineering, University of the Peloponnese, Tripoli, Greece*

Received 1 December 2021; received in revised form 2 March 2022; accepted 5 April 2022
Available online 14 April 2022

Abstract

An incompressible, electrically conducting Biomagnetic Fluid Dynamics (BFD) flow—namely the flow of blood with magnetic particles through a two-dimensional stretching cylinder under the influence of a magnetic dipole—is numerically and theoretically investigated in the present study. Herein, fluid viscosity and thermal conductivity are supposed to vary as an inverse function and as linear functions of temperature, respectively. This study involves two areas of analysis, namely magnetohydrodynamics (MHD) and ferrohydrodynamics (FHD). The basic blood flow features when magnetic particles are added to blood, as well as those of pure blood are discussed. Using a similarity approach, the governing system of partial differential equations are converted into a system of ordinary differential equations which are solved numerically by considering an efficient technique based on a common finite differences method, consisting of central differencing, tridiagonal matrix manipulation and an iterative procedure. The significant effects of various physical non-dimensional parameters concerning the axial velocity, temperature, skin friction coefficient and rate of heat transfer are demonstrated graphically. The obtained results reveal that with increasing values of the ferromagnetic interaction parameter, the magnetic field parameter, the thermal conductivity parameter and the viscosity variation parameter, fluid (blood-Fe_3O_4) velocity is reduced, whereas both axial velocity and temperature are enhanced for the curvature parameter. Both the skin friction coefficient and the rate of heat transfer decline with rising values of the thermal conductivity parameter. To make the results physically reliable, a temporal stability analysis is also provided in this study. Finally, the accuracy of the applied numerical technique is validated with existing published literature for some limiting cases, and the results are found to be in excellent agreement. The present outcomes disclose that the behavior of blood flow can be controlled by employing a strong magnetic field. It is hoped that such kind of results will be useful in medical sector especially in MRI, magnetic drug targeting and magnetic hyperthermia treatments.

Keywords: Biomagnetic fluid; Blood; Magnetic particles; Variable fluid viscosity; Thermal conductivity; Magnetohydrodynamics; Ferrohydrodynamics; Stretched cylinder; Magnetic dipole

* Corresponding author.
E-mail address: etzirtzilakis@uop.gr (E.E. Tzirtzilakis).

https://doi.org/10.1016/j.matcom.2022.04.008

Nomenclature

(u, v)	Velocity components [m/s]
(x, r)	Components of the Cartesian system[m]
δ	Constant
R	Radius of the cylinder [m]
c	Distance between the magnetic dipole to sheet [m]
L	Characteristic length [m]
U_0	Referred velocity [m/s]
H	Magnetic field of strength [A/m]
T	Fluid temperature [K]
T_w	Temperature of the sheet [K]
T_c	Curie temperature (Fluid temperature far away from the sheet) [K]
M_1	Fluid magnetization [A/m]
M	Magnetic field parameter
B	Magnetic induction
$U(x)$	Stretched velocity [m/s]
C_p	Specific heat at constant pressure [J kg^{-1} K^{-1}]
$f^{'}$	Dimensionless velocity component in x-direction
γ	Strength of magnetic field at the source position.
K	Pyromagnetic coefficient [K^{-1}]
D	Curvature parameter
a	Thermal conductivity parameter
Pr	Prandtl number
Nu_x	Rate of heat transfer
C_f	Skin friction coefficient
Re	Local Reynolds number
t	Time [s]

Greek symbols

η , τ	Dimensionless coordinates
θ	Dimensionless temperature
$\theta^{'}(0)$	Wall heat transfer gradient
ψ	Stream function
φ	Volume fraction
ρ	Fluid density [kg/m^3]
μ	Dynamic viscosity [kg/ms]
μ^*	Constant values of the coefficient of the fluid viscosity
μ_0	Magnetic fluid permeability [NA^{-2}]
υ	Kinematical viscosity [m^2/s]
σ	Electrical conductivity [S/m]
ε_1	Convergence criteria
ε	Dimensionless Curie temperature
λ	Viscous dissipation parameter
β	Ferromagnetic interaction parameter
θ_r	Viscosity variation parameter
ω	Eigen value parameter

α	Dimensionless distance
κ	Thermal conductivity [J/m s K]
κ^*	Constant values of the coefficient of the fluid viscosity
τ_w	Wall shear stress

List of abbreviations

BFD	Biomagnetic Fluid Dynamics
FHD	FerroHydroDynamics
MHD	MagnetoHydroDynamics
PDEs	Partial Differential Equations
ODEs	Ordinary Differential Equations

Subscripts symbol

$()_{mf}$	Indicates magnetic fluid
$()_f$	Represent base fluid
$()_s$	Means magnetic particles (solid particles)

Superscripts symbol

$()'$	Differentiation with respect to η

1. Introduction

In recent decades in the biomedical and bioengineering sectors, different types of magnetic particles with biological fluid have gained serious attention from researchers because of their numerous applications such as in magnetic resonance imaging (MRI), cancer therapy (hyperthermia), magnetic drug, gene delivery and magnetic separation [10,11,15,24,33,40] due to their biocompatibility, biodegradability and ease of synthesis, providing abundant functions for specific applications. In fluid mechanics, Biomagnetic Fluid Dynamics (BFD) is a comparatively new area of study, in which the action of a strong applied magnetic field is investigated on biological fluids, and blood is one of the prominent examples of a biomagnetic fluid. Essentially, this new area involves the principles of magnetohydrodynamics (MHD) and ferrohydrodynamics (FHD). In MHD, fluids are assumed to be electrically conducting and the influence of magnetization/polarization is ignored, whereas in FHD, the fluid flow is influenced by the polarization force arising due to the presence of fluid magnetization, and fluid is treated as an electrically non-conducting fluid.

Considering the principles of ferrohydrodynamics (FHD), Haik et al. [16] were the first to deliver the idea of a mathematical model of BFD, in which fluids were assumed to be Newtonian and electrically non-conducting, showing in their studies that fluid flow had a great influence on the presence of high-gradient magnetic fields. Later, Tzirtzilakis [42] developed a BFD model, namely, a blood model considering the combined principles of MHD and FHD. Recently, Murtaza et al. [30] provided a BFD study including the ideas of MHD and FHD. They found that in terms of the velocity profile, the BFD formulation produces significantly reduced results compared to those of the MHD or FHD separate formulations, whereas in terms of the temperature profile, the reverse behavior is found. An incompressible, electrically conducting blood model through a stretching cylinder, as presented by Ferdows et al. [12] and this study, also combined the principles of MHD and FHD. Siddiqa et al. [38] investigated the thermal radiation therapy in the presence of a localized magnetic field in relation to biomagnetic fluid flow. Rajashekhar et al. [35] analyzed a blood flow model on two regions of a cylindrical surface, one of which was considered as a magnetic region and the other as a non-magnetic region, and this model was based on the principles of FHD. They found that in the magnetic region, blood flow was remarkably reduced compared to the non-magnetic region. The effects of variable fluid viscosity on biomagnetic fluid flow and heat transfer over a two-dimensional non-linear stretching sheet were studied by Alam et al. [3]. The researchers found that blood flow decreased with increasing values of the viscosity variation parameter.

A theoretical and mathematical study of Carreau type fluid model where fluid assumed as non-Newtonian, through a nonlinear stretching sheet in presence of temperature dependent thermal conductivity and thermal radiation analyzed by Megahed [26]. Abbas et al. [1] have discussed the effects of thermal dependent viscosity and conductivity on steady Powell–Eyring fluid over a stratified stretching sheet in porous medium. In this study investigators found that the impact of thermal radiation on fluid temperature profile are more significant than that on the velocity distribution. Using shooting method, Megahed et al. [27] analyzed the unsteady MHD fluid flow model over a stretching sheet in the presence of heat flux. Moreover, this study was also extended considering fluid viscosity and thermal conductivity as temperature dependent. The impacts of viscosity and thermal conductivity on MHD convective flow through a non-isothermal vertical surface in porous medium in the presence of viscous dissipative heat and thermal radiation have obtained by Hazarika et al. [18]. Finally, a comprehensive study of blood flow through a stretching sheet in the presence of magnetic dipole and thermal radiation studied by Alam et al. [5].

In 1995, the term nanofluid was first introduced by Choi [9], who showed that the mixing of a base fluid with nanoparticles enhanced the fluid properties, mainly the thermal conductivity. Recently, Hazarika et al. [19] analyzed a numerical solution of $C_2H_6O_2$ based nanofluid flow in a vertical channel by utilizing MATLAB code, where nanoparticles are in platelet shape and Al_2O_3 and TiO_2 particles are considered. The importance of these metal oxide nanoparticles is found in pharmaceutical areas and biomedical engineering. The shape effect on graphene–water nanofluid in a two-dimensional Marangoni boundary layer under the influence of suction and thermal radiation was discussed by Rahid et al. [34]. Alam et al. [4] examined the blood-Au nanofluid flow in the presence of a magnetic dipole over a two-dimensional stretching sheet and consequently both principles of MHD and FHD were also adopted in the considered BFD flow. In that study, they showed how nanoparticles were influenced when mixed with base fluids such as blood and found that blood velocity was significantly enhanced in case of the blood-Au mixture rather than pure blood, and the opposite effect was found in terms of the temperature profile. Abdi et al. [2] studied the magnetic fluid flow, considering water as the base fluid and with Fe_3O_4 used for the magnetic particles in the turbulence region. Investigations of MHD nanofluid flow and heat transfer in a microchannel can be found in the study of Karimipour et al. [22], in which two types of nanoparticles were used—namely, Au and Al_2O_3—and water was used as a base fluid. Ali et al. [6] proposed a time fractional model, where Brinkman-type fluid (blood) with magnetic particles was examined in a heated cylindrical tube. With the aid of Laplace and Hankel's transforms, exact solutions were found, and they showed that the magnetic field controlled the blood velocity, and this was more pronounced when the values of the magnetics were large. The effects of velocity and thermal slipping on H_2O-Ag nanofluid over a two-dimensional stretching cylinder were investigated by Mishra et al. [28], in which two types of models were considered for different shapes—one was spherical and the other was cylindrical. They found that in both cases, the temperature profile was enhanced by increasing the volume fraction. Amer Qureshi [7] examined non-Newtonian two-dimensional Williamson nanofluids, i.e., Cu–water and TiO_2-water, over a stretching sheet in the presence of velocity slip effects, in which the thermal conductivity of the fluid was assumed as a linear function of temperature. The effects of variable fluid viscosity and thermal conductivity on MHD Casson nanofluid flow over a vertical flat plate were studied by Gbadeyan et al. [14]. Hussain [20] investigated the effects of variable fluid viscosity on an MHD hybrid nanofluid, subject to homogeneous–heterogeneous reactions. Mohamed et al. [8] analyzed the MHD boundary layer fluid flow, considering water as a base fluid and magnetic particles assumed as nanoparticles (i.e., magnetite, Cobalt ferrite, Mn-Zn ferrite) over a two-dimensional flat plate under the influence of thermal radiation.

Based on the above-mentioned studies, to the authors knowledge, the numerical as well as the theoretical BFD flow with magnetic particles over a two-dimensional stretching cylinder subject to no-slip boundary conditions has not yet been investigated. The mathematical model used is that of the extended BFD which incorporates both MHD and FHD formulations. Moreover, the fluid viscosity and thermal conductivity are assumed as inverse and linear function of temperature, respectively. The governing set of partial differential equations subject to corresponding boundary conditions is transformed into ordinary differential equations using the usual similarity transformations. The numerical solution is attained by applying an efficient technique which is based on a common finite difference method with central differencing, tridiagonal matrix manipulation and an iterative procedure. To make the results more physically reliable, a theoretical stability analysis has also been performed. The important behavior of appearing physical parameters such as ferromagnetic interaction parameter, magnetic field parameter, magnetic particles volume fraction, curvature parameter, thermal conductivity, variable viscosity etc. on the velocity and temperature profile, as well as the skin friction coefficient and the rate of heat transfer, are discussed in detail,

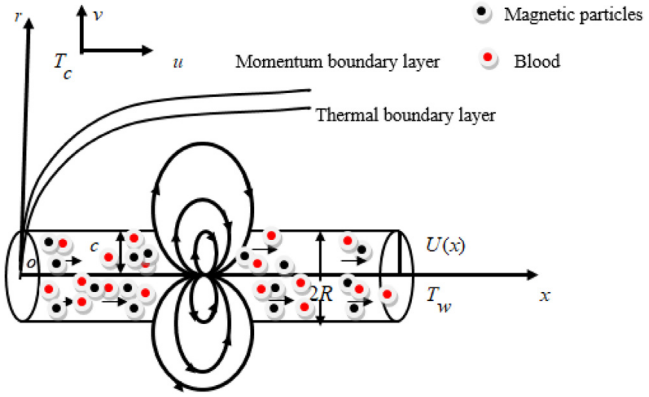

Fig. 1. Schematic diagram of the flow problem [6].

considering the cases of pure blood and blood with Fe_3O_4 nanoparticles. It is hope that the present study will help in understanding the basic mechanism for applications in biomedicine and bioengineering such as separation of targeted molecules, magnetic drug targeting, diagnostic techniques, hyperthermia, or hypothermia treatment etc.

2. Mathematical analysis with flow geometry

The flow of an electrically biomagnetic fluid (blood) with magnetic particles stretched with velocity $U(x) = \frac{U_0 x}{L}$, where U_0 is a positive constant and L is a characteristic length along a two-dimensional stretching cylinder of radius R, is considered in this study. The x-axis is considered to be along the cylinder and the r-axis is normal to the cylinder, as demonstrated in Fig. 1. The temperature of the ambient fluid is considered as T_c situated far away from the sheet, and T_w is the surface temperature, where $T_w < T_c$. A magnetic field of strength H is generated by a magnetic dipole on the center of the r axis at distance c from the sheet.

Considering the above assumptions, we expand upon the ideas of [39] and the governing continuity, momentum and energy equations associated with the applicable boundary conditions are expressed in the following form [12,30,39,42]:

$$\frac{\partial}{\partial x}(ru) + \frac{\partial}{\partial r}(rv) = 0 \tag{1}$$

$$u\frac{\partial u}{\partial x} + v\frac{\partial u}{\partial r} = \frac{1}{\rho_{mf}}\frac{1}{r}\frac{\partial}{\partial r}\left[\mu_{mf}\left(r\frac{\partial u}{\partial r}\right)\right] - \frac{\sigma_{mf}}{\rho_{mf}}B^2 u + \frac{\mu_0}{\rho_{mf}}M_1\frac{\partial H}{\partial x} \tag{2}$$

$$\left(\rho C_{\mathrm{p}}\right)_{\mathrm{mf}}\left(\mathrm{u}\frac{\partial \mathrm{T}}{\partial \mathrm{x}} + \mathrm{v}\frac{\partial \mathrm{T}}{\partial \mathrm{r}}\right) + \mu_0 \mathrm{T}\frac{\partial \mathrm{M}_1}{\partial \mathrm{T}}\left(\mathrm{u}\frac{\partial \mathrm{H}}{\partial \mathrm{x}} + \mathrm{v}\frac{\partial \mathrm{H}}{\partial \mathrm{r}}\right) = \frac{1}{\mathrm{r}}\frac{\partial}{\partial \mathrm{r}}\left[\kappa^*_{\mathrm{mf}}\left(\mathrm{r}\frac{\partial \mathrm{T}}{\partial \mathrm{r}}\right)\right] \tag{3}$$

Subject to the boundary conditions [39]:

$$r = R : u = U(x),\ v = 0,\ T = T_w \tag{4}$$

$$r \to \infty : u \to 0,\ T \to T_c \tag{5}$$

Here, in the x and r directions the velocity components are denoted by the symbols u and v, respectively. Furthermore, the symbols in the above equations ρ, σ, μ, C_p, κ, μ_0, H, M_1 denote biomagnetic fluid (blood) density, electrical conductivity, dynamic viscosity, specific heat at constant pressure, thermal conductivity, magnetic permeability, magnetic field strength and magnetization, respectively. The subscript symbol $()_{mf}$ indicates the magnetic fluid. Furthermore, B symbolizes the magnetic induction, where $B = \mu_0 H$. The term $\sigma_{mf} B^2 u$ represents the Lorentz force per unit volume, which acts along the x direction and is known as MHD [29,30]. The third term on the right-hand side of Eq. (2), i.e., $\mu_0 M_1 \frac{\partial H}{\partial x}$, represents the components of the ferromagnetic body force per unit volume, which depend on the existence of a magnetic gradient in the x direction, whereas the terms in the

energy equation $\mu_0 T \frac{\partial M_1}{\partial T}\left(u\frac{\partial H}{\partial x}+v\frac{\partial H}{\partial r}\right)$ in (3) account for heating due to adiabatic magnetization, and according to [16,18,42–44], these terms are well known in the area of FHD.

According to [32,41,43,44], the magnetic dipole gives rise to a magnetic field that is sufficiently strong to saturate the biofluid and its scalar potential, given by

$$V=\frac{\alpha}{2\pi}\frac{x}{x^2+(r+c)^2} \tag{6}$$

Here, α is a dimensionless distance and $\alpha=\gamma$ where γ is the strength of the magnetic field.

Therefore, the magnitude of the magnetic field of intensity, i.e., $\left\|\overrightarrow{\mathrm{H}}\right\|=\mathrm{H}$, is given by

$$\mathrm{H}\,(\mathrm{x},\mathrm{r})=\left[\mathrm{H}_{\mathrm{x}}^2+\mathrm{H}_{\mathrm{r}}^2\right]^{\frac{1}{2}}=\frac{\gamma}{2\pi}\frac{\mathrm{x}^2}{\mathrm{x}^2+(\mathrm{r}+\mathrm{c})^2} \tag{7}$$

and H_x , H_r are the components of the magnetic field $\overrightarrow{H}=(H_x\,,H_r)$, given by

$$H_x(x,r)=-\frac{\partial V}{\partial x}=\frac{\gamma}{2\pi}\frac{x^2-(r+c)^2}{\left(x^2+(r+c)^2\right)^2} \tag{8}$$

$$H_r\ (x,r)=-\frac{\partial V}{\partial r}=\frac{\gamma}{2\pi}\frac{2x\,(r+c)}{\left(x^2+(r+c)^2\right)^{\,2}} \tag{9}$$

According to the previous studies of analogous manipulations of Eqs. (8) and (9), these take the following form:

$$\frac{\partial H}{\partial x}=-\frac{\gamma}{2\pi}\frac{2x}{(r+c)^4} \tag{10}$$

$$\frac{\partial H}{\partial r}=-\frac{\gamma}{2\pi}\left(\frac{-2}{(r+c)^3}+\frac{4x^2}{(r+c)^5}\right) \tag{11}$$

Thus, the magnetic field intensity H can be expressed as

$$H\,(x,r)=\frac{\gamma}{2\pi}\left(\frac{1}{(r+c)^2}-\frac{x^2}{(r+c)^4}\right) \tag{12}$$

The variation of magnetization M_1 with temperature T is defined by a linear relation [41–43]

$$M_1=K\,(T_c-T) \tag{13}$$

Following the studies of Salawu and Dada [37], fluid viscosity and thermal conductivity are assumed to be temperature-dependent, where fluid viscosity is an inverse function of temperature and thermal conductivity takes a linear form and is mathematically defined as:

$$\frac{1}{\mu_{mf}}=\frac{[1+\delta\,(T_c-T)]}{\mu_{mf}^*} \tag{14}$$

Furthermore, the thermal conductivity is expressed as:

$$\kappa_{mf}^*=\kappa_{mf}\ (1+a\theta) \tag{15}$$

Where α is the thermal conductivity and δ is a constant. Furthermore, the symbols μ_{mf}^* and κ_{mf} indicate the constant values of the coefficient of fluid viscosity and the thermal conductivity of the biomagnetic fluid.

The physical parameters of the magnetic fluid are considered as previously studied by Makinde [25], and these take the following form:

$$\begin{aligned}&\mu_{mf}^*=\mu_f(1-\varphi)^{-2.5},(\rho C_p)_{mf}=(1-\varphi)(\rho C_p)_f+\varphi(\rho C_p)_s,\\&\rho_{mf}=(1-\phi)\rho_f+\phi\rho_s\end{aligned} \tag{16}$$

$$\frac{\sigma_{mf}}{\sigma_f}=1+\frac{3\left(\frac{\sigma_s}{\sigma_f}-1\right)\varphi}{\left(\frac{\sigma_s}{\sigma_f}+1\right)-\left(\frac{\sigma_s}{\sigma_f}-1\right)\varphi},\ \frac{\kappa_{mf}}{\kappa_f}=\frac{(\kappa_s+2\kappa_f)-2\phi(\kappa_f-\kappa_s)}{(\kappa_s+2\kappa_f)+\phi(\kappa_f-\kappa_s)} \tag{17}$$

Here, φ indicates the volume fraction of the magnetic particles, whereas $\varphi = 0$ corresponds to the regular fluid. Note that the subscript symbols $()_f$ and $()_s$ signify the base fluid (blood) and magnetic particles (Fe_3O_4), respectively.

3. Transformation of equations

To make the set of Eqs. (1)–(3), associated with boundary conditions (4) and (5), into dimensionless equations the following non-dimensional coordinates are introduced [39]:

$$\eta = \frac{r^2 - R^2}{2R}\left(\frac{U}{\vartheta_f x}\right)^{\frac{1}{2}}, \quad \psi = \sqrt{U\vartheta_f x}\, Rf(\eta), \quad \theta(\eta) = \frac{T_c - T}{T_c - T_w} \tag{18}$$

Now, the continuity equation can be satisfied automatically when the velocity components are defined in the following way:

$$\begin{aligned} u &= \frac{1}{r}\frac{\partial \psi}{\partial r} \\ v &= -\frac{1}{r}\frac{\partial \psi}{\partial x} \end{aligned} \tag{19}$$

By implementing equations (18) and (19) into the momentum and energy equations, i.e., (2) and (3), we obtain the following system of ordinary differential equations:

$$\begin{aligned} &(1 + 2\eta\,\mathrm{D})\,\mathrm{f}''' + 2\mathrm{D}\,\mathrm{f}'' - \frac{\theta'}{\theta - \theta_\mathrm{r}}(1 + 2\eta\,\mathrm{D})\,\mathrm{f}'' + \frac{\theta - \theta_\mathrm{r}}{\theta_\mathrm{r}}(1-\phi)^{2.5}\left[1 + \frac{3\left(\frac{\sigma_\mathrm{s}}{\sigma_\mathrm{f}} - 1\right)\phi}{\left(\frac{\sigma_\mathrm{s}}{\sigma_\mathrm{f}} + 1\right) - \left(\frac{\sigma_\mathrm{s}}{\sigma_\mathrm{f}} - 1\right)\phi}\right]\mathrm{M}\,\mathrm{f}' \\ &+ \frac{\theta - \theta_\mathrm{r}}{\theta_\mathrm{r}}(1-\phi)^{2.5}\left(1 - \phi + \phi\frac{\rho_\mathrm{s}}{\rho_\mathrm{f}}\right)\left(\mathrm{f}'^2 - \mathrm{f}\,\mathrm{f}''\right) + \frac{\theta - \theta_\mathrm{r}}{\theta_\mathrm{r}}(1-\phi)^{2.5}\frac{2\beta\theta}{(\eta + \alpha)^4} = 0 \end{aligned} \tag{20}$$

$$\begin{aligned} &(1 + \mathrm{a}\theta)\,(1 + 2\eta D)\,\theta'' + 2\mathrm{D}\,(1 + \mathrm{a}\theta)\,\theta' + (1 + 2\eta D)\,\mathrm{a}\theta'^2 + \frac{\kappa_\mathrm{f}}{\kappa_\mathrm{mf}}\left(1 - \phi + \phi\frac{(\rho C_\mathrm{p})_\mathrm{s}}{(\rho C_\mathrm{p})_\mathrm{f}}\right)\mathrm{Pr}\,\mathrm{f}\theta' \\ &+ \frac{\kappa_\mathrm{f}}{\kappa_\mathrm{mf}}\frac{2\beta\lambda\mathrm{f}(\theta - \varepsilon)}{(\eta + \alpha)^3} = 0 \end{aligned} \tag{21}$$

Along with boundary conditions:

$$\eta = 0 : f = 0,\ f' = 1,\ \theta = 1 \tag{22}$$

$$\eta \to \infty : f' \to 0, \theta \to 0 \tag{23}$$

In the above set of ordinary differential equations the dimensionless parameters are: the ferromagnetic interaction parameter $\beta = \frac{\gamma}{2\pi}\frac{\mu_0 K(T_c - T_w)\rho_f}{\mu_f^2}$; the viscous dissipation parameter $\lambda = \frac{u_0\mu_f^2}{L\kappa_f(T_c - T_w)\rho_f}$; the Curie temperature $\varepsilon = \frac{T_c}{T_c - T_w}$; the curvature parameter $D = \left(\frac{L\upsilon_f}{u_0 R^2}\right)^{\frac{1}{2}}$; the dimensionless distance $\alpha = \left(\frac{\mathrm{u}_0}{\mathrm{L}\upsilon_\mathrm{f}}\right)^{\frac{1}{2}}\mathrm{c}$; the Prandtl number $\mathrm{Pr} = \frac{(\mu C_p)_f}{\kappa_f}$; the magnetic field parameter $M = \frac{\sigma_f \mu_0^2 H^2 L}{u_0}$; and the viscosity variation parameter $\theta_r = -\frac{1}{\delta(T_c - T_w)}$, where for liquids the value of θ_r is negative and for gases θ_r is positive.

The most important characteristic of the present analysis from the engineering point of view is to study the skin friction coefficient and the rate of heat transfer, which are mathematically defined by

$$C_f = \frac{2\tau_w}{\rho_f U^2} \text{ and } Nu_x = \frac{x q_w}{\kappa_f\,(\mathrm{T_c} - \mathrm{T_w})} \tag{24}$$

where τ_w and Nu_x represent the local shear stress and heat transfer from the surface, respectively, and are defined in following way:

$$\tau_w = \mu_{mf}\left(\frac{\partial u}{\partial r}\right)_{r=R} \text{ and } q_w = \kappa_{mf}\left(\frac{\partial T}{\partial r}\right)_{r=R} \tag{25}$$

Using (25), Eq. (24) can be expressed in the following form:

$$C_f\,\mathrm{Re}^{\frac{1}{2}} = \frac{2}{(1-\varphi)^{2.5}} f''(0) \tag{26}$$

$$Nu_x \,\mathrm{Re}^{-\frac{1}{2}} = -\frac{\kappa_{mf}}{\kappa_f}\theta'(0) \tag{27}$$

Here, $\mathrm{Re} = \frac{U_x}{\upsilon_f}$ indicates the local Reynolds number.

4. Stability analysis

Following the studies of Ferdows et al. [13] and Murtaza et al. [31], to perform the stability analysis in the present model, we need to express this model in an unsteady form, and this can be written in the following way

$$\frac{\partial u}{\partial t} + u\frac{\partial u}{\partial x} + v\frac{\partial u}{\partial r} = \frac{1}{\rho_{mf}}\frac{1}{r}\frac{\partial}{\partial r}\left[\mu_{mf}\left(r\frac{\partial u}{\partial r}\right)\right] - \frac{\sigma_{mf}}{\rho_{mf}}B^2u + \frac{\mu_0}{\rho_{mf}}M_1\frac{\partial H}{\partial x} \tag{28}$$

$$\left(\rho C_p\right)_{mf}\left(\frac{\partial T}{\partial t} + u\frac{\partial T}{\partial x} + v\frac{\partial T}{\partial r}\right) + \mu_0 T\frac{\partial M_1}{\partial T}\left(u\frac{\partial H}{\partial x} + v\frac{\partial H}{\partial r}\right) = \frac{1}{r}\frac{\partial}{\partial r}\left[\kappa_{mf}\left(r\frac{\partial T}{\partial r}\right)\right] \tag{29}$$

where time is represented by the symbol t and the new similarity transformations are:

$$\begin{aligned}&\eta = \frac{r^2 - R^2}{2R}\left(\frac{u_0}{\vartheta_f L}\right)^{\frac{1}{2}},\ u = \frac{u_0 x}{L}\frac{\partial f\,(\eta,\tau)}{\partial \eta}, v = -\frac{R}{r}\sqrt{\frac{u_0\upsilon_f}{L}}f\,(\eta\,,\,\tau)\,;\\ &\theta\,(\eta\,,\,\tau) = \frac{T_c - T}{T_c - T_w},\ \tau = \frac{u_0 t}{L}\end{aligned} \tag{30}$$

By introducing new similarity variables, Eqs. (28)–(29) are reduced in the form given below:

$$\begin{aligned}&(1+2\eta\,D)\frac{\partial^3 f}{\partial \eta^3} + 2D\frac{\partial^2 f}{\partial \eta^2} - \frac{1}{\theta - \theta_r}(1+2\eta D)\frac{\partial^2 f}{\partial \eta^2}\frac{\partial \theta}{\partial \eta} + \frac{\theta - \theta_r}{\theta_r}(1-\varphi)^{2.5}\\ &\left[1 + \frac{3\left(\frac{\sigma_s}{\sigma_f} - 1\right)\varphi}{\left(\frac{\sigma_s}{\sigma_f} + 1\right) - \left(\frac{\sigma_s}{\sigma_f} - 1\right)\varphi}\right]M\frac{\partial f}{\partial \eta} + \frac{\theta - \theta_r}{\theta_r}(1-\varphi)^{2.5}\left(1 - \varphi + \varphi\frac{\rho_s}{\rho_f}\right)\\ &\left[\frac{\partial^2 f}{\partial \eta \partial \tau} + \left(\frac{\partial f}{\partial \eta}\right)^2 - f\frac{\partial^2 f}{\partial \eta^2}\right] + \frac{\theta - \theta_r}{\theta_r}(1-\varphi)^{2.5}\frac{2\beta\theta}{(\eta+\alpha)^4} = 0\end{aligned} \tag{31}$$

$$\begin{aligned}&(1+a\theta)\,(1+2\eta D)\frac{\partial^2 \theta}{\partial \eta^2} + \,2\mathrm{D}\,(1+a\theta)\frac{\partial \theta}{\partial \eta} + (1+2\eta D)\,a\left(\frac{\partial \theta}{\partial \eta}\right)^2 + \frac{\kappa_f}{\kappa_{mf}}\left(1 - \varphi + \varphi\frac{\left(\rho C_p\right)_s}{\left(\rho C_p\right)_f}\right)\\ &\qquad \mathrm{Pr}\left[f\frac{\partial \theta}{\partial \eta} - \frac{\partial \theta}{\partial \tau}\right] + \frac{\kappa_f}{\kappa_{mf}}\frac{2\beta\lambda f\,(\theta - \varepsilon)}{(\eta+\alpha)^3} = 0\end{aligned} \tag{32}$$

With the transformed boundary conditions:

$$f\,(0,\,\tau) = 0, \frac{\partial f\,(0,\,\tau)}{\partial \eta} = 1,\ \theta\,(0,\,\tau) = 1 \tag{33}$$

$$\frac{\partial f\,(\infty,\,\tau)}{\partial \eta} \to 0, \theta\,(\infty,\,\tau) \to 0 \tag{34}$$

According to Weidman et al. [46], the governing set of ordinary differential equations (20)–(21), along with boundary conditions (22) and (23), are expressed as stabilized steady flow solutions by writing the following scheme:

$$f\,(\eta\,,\,\tau) = f_0\,(\eta) + e^{-\omega\tau}F\,(\eta,\,\tau)\,, \theta\,(\eta\,,\,\tau) = \theta_0\,(\eta) + e^{-\omega\tau}G\,(\eta\,,\,\tau) \tag{35}$$

The symbol ω represents the eigenvalue parameter in the set of equations $\omega_1 < \omega_2 < \omega_3 < \cdots \ldots < \omega_n$, where the flow is stable if the values of $\omega_1 > 0$ and the opposite happens, i.e., the initial growth of a disturbance occurs, if $\omega_1 < 0$. Consequently, it is assumed that $F\,(\eta,\,\tau)$ and $G\,(\eta\,,\,\tau)$ are small compared to $f\,(\eta) = f_0\,(\eta)$ and

$\theta(\eta) = \theta_0(\eta)$. After introducing (35) into (31) and into (34), it is obtained that:

$$(1+2\eta D)\frac{\partial^3 F}{\partial \eta^3} + 2D\frac{\partial^2 F}{\partial \eta^2} - (1+2\eta D)\left[\frac{f_0'}{G}\frac{\partial G}{\partial \eta} + \frac{\theta_0'}{G}\frac{\partial^2 F}{\partial \eta^2}\right] + (1-\varphi)^{2.5}$$
$$\left[1 + \frac{3\left(\frac{\sigma_s}{\sigma_f} - 1\right)\varphi}{\left(\frac{\sigma_s}{\sigma_f} + 1\right) - \left(\frac{\sigma_s}{\sigma_f} - 1\right)\varphi}\right] MG\frac{\partial F}{\partial \eta} + (1-\varphi)^{2.5}\left(1 - \varphi + \varphi\frac{\rho_s}{\rho_f}\right) \tag{36}$$
$$\left[G\frac{\partial^2 F}{\partial \eta \partial \tau} - \omega\frac{\partial F}{\partial \eta} + 2f_0'\frac{\partial F}{\partial \eta} - f_0\frac{\partial^2 F}{\partial \eta^2} - Ff_0''\right] + (1-\varphi)^{2.5}\frac{2\beta G^2}{(\eta+\alpha)^4} = 0$$

$$(1+aG)\,(1+2\eta D)\frac{\partial^2 G}{\partial \eta^2} + 2\mathrm{D}\,(1+aG)\frac{\partial G}{\partial \eta} + 2a\,(1+2\eta D)\,\theta_0\frac{\partial G}{\partial \eta} +$$
$$\frac{\kappa_f}{\kappa_{mf}}\left(1 - \varphi + \varphi\frac{(\rho C_p)_S}{(\rho C_p)_f}\right)\mathrm{Pr}\left[f_0\frac{\partial G}{\partial \eta} + F\theta_0' - \frac{\partial G}{\partial \tau} + \omega G\right] - \frac{\kappa_f}{\kappa_{mf}}\frac{2\beta\lambda F\varepsilon}{(\eta+\alpha)^3} + \tag{37}$$
$$\frac{\kappa_f}{\kappa_{mf}}\frac{2\beta\lambda\,(f_0 G + F\theta_0)}{(\eta+\alpha)^3} = 0$$

and the boundary conditions are:

$$F(0,\,\tau) = 0,\ \frac{\partial F(0,\,\tau)}{\partial \eta} = 1,\ G(0,\,\tau) = 1 \tag{38}$$

$$\frac{\partial F(\infty,\,\tau)}{\partial \eta} \to 0,\ G(\infty,\,\tau) \to 0 \tag{39}$$

Now, to find the stabilization of the initial growth or decay of the disturbance of the steady-state flow solutions, it is set $\tau = 0$, as well as $F(\eta,\,\tau) = F_0(\eta)$, $G(\eta,\,\tau) = G_0(\eta)$ and hereby the following form of the values of the linearized eigenvalue is derived:

$$(1+2\eta\,D)\,F_0''' + 2DF_0'' - (1+2\eta D)\left[\frac{f''G_0'}{G_0} + \frac{\theta_0' F_0'^2}{G_0}\right] + (1-\varphi)^{2.5}$$
$$\left[1 + \frac{3\left(\frac{\sigma_S}{\sigma_f} - 1\right)\varphi}{\left(\frac{\sigma_S}{\sigma_f} + 1\right) - \left(\frac{\sigma_S}{\sigma_f} - 1\right)\varphi}\right] M\,G_0F_0' + (1-\varphi)^{2.5}\left(1 - \varphi + \varphi\frac{\rho_S}{\rho_f}\right) \tag{40}$$
$$\left[2f_0'G_0F_0' - \omega G_0F_0' - f_0G_0F_0'' - F_0G_0f_0''\right] + (1-\varphi)^{2.5}\frac{2\beta G_0^2}{(\eta+\alpha)^4} = 0$$

$$(1+aG_0)\,(1+2\eta D)\,G_0'' + 2\mathrm{D}\,(1+aG_0)\,G_0' + 2a\,(1+2\eta D)\,\theta_0 G' + \frac{\kappa_f}{\kappa_{mf}}\left(1 - \varphi + \varphi\frac{(\rho C_P)_S}{(\rho C_P)_f}\right)$$
$$\mathrm{Pr}\left[f_0G_0' + F\theta_0' + \omega\,G_0\right] - \frac{\kappa_f}{\kappa_{mf}}\frac{2\beta\lambda F_0\varepsilon}{(\eta+\alpha)^3} + \frac{\kappa_f}{\kappa_{mf}}\frac{2\beta\lambda\,(f_0G_0 + F_0\theta_0)}{(\eta+\alpha)^3} = 0 \tag{41}$$

subject to the boundary conditions:

$$F(0) = 0,\ F_0'(0) = 0,\ G_0(0) = 0 \tag{42}$$

$$F_0'(\eta) \to 0,\ G_0(\eta) \to 0 \text{ as } \eta \to \infty \tag{43}$$

Following the studies of Harris et al. [17], the smallest values of the eigenvalues can be found if one can relax the boundary conditions $F_0'(\eta) \to 0$ as $\eta \to \infty$ into $F_0''(0) = 1$, **a**nd this takes the following form:

$$F(0) = 0,\ F_0'(0) = 0,\ G_0(0) = 0,\ F_0''(0) = 1 \tag{44}$$

$$G_0(\infty) \to 0 \tag{45}$$

5. Numerical procedure

According to the study of Kafoussias and Williams [21], this model can be solved numerically by applying an approximate technique that has better stability characteristics than the classical Runge–Kutta combined shooting method. Moreover, is simple, accurate and efficient and it is based on three common essential features. This technique is based on (i) the common finite difference method with central differencing, (ii) tridiagonal matrix

manipulation, and finally, (iii) an iterative procedure. According to this study, the momentum Eq. (20) can be expressed as:

$$(1+2\eta D)\, f''' + \left[2D - \frac{\theta'}{\theta-\theta_r}(1+2\eta D) - \frac{\theta-\theta_r}{\theta_r}(1-\varphi)^{2.5}\left(1-\varphi+\varphi\frac{\rho_S}{\rho_f}\right) f\right] f'' + \left[\frac{\theta-\theta_r}{\theta_r}(1-\varphi)^{2.5}\left[1+\frac{3\left(\frac{\sigma_S}{\sigma_f}-1\right)\varphi}{\left(\frac{\sigma_S}{\sigma_f}+1\right)-\left(\frac{\sigma_S}{\sigma_f}-1\right)\varphi}\right] M + \frac{\theta-\theta_r}{\theta_r}(1-\varphi)^{2.5}\left(1-\varphi+\varphi\frac{\rho_S}{\rho_f}\right) f'\right] f' - \frac{\theta-\theta_r}{\theta_r}(1-\varphi)^{2.5}\frac{2\beta\theta}{(\eta+\alpha)^4} = 0 \tag{46}$$

This Eq. (46) is expressed as a second-order ordinary differential equation by setting $y(x) = f'(\eta)$ and we have,

$$(1+2\eta D)\left(f'\right)'' + \left[2D - \frac{\theta'}{\theta-\theta_r}(1+2\eta D) - \frac{\theta-\theta_r}{\theta_r}(1-\varphi)^{2.5}\left(1-\varphi+\varphi\frac{\rho_S}{\rho_f}\right) f\right]\left(f'\right)' + \left[\frac{\theta-\theta_r}{\theta_r}(1-\varphi)^{2.5}\left[1+\frac{3\left(\frac{\sigma_S}{\sigma_f}-1\right)\varphi}{\left(\frac{\sigma_S}{\sigma_f}+1\right)-\left(\frac{\sigma_S}{\sigma_f}-1\right)\varphi}\right] M + \frac{\theta-\theta_r}{\theta_r}(1-\varphi)^{2.5}\left(1-\varphi+\varphi\frac{\rho_S}{\rho_f}\right) f'\right] f' = \frac{\theta-\theta_r}{\theta_r}(1-\varphi)^{2.5}\frac{2\beta\theta}{(\eta+\alpha)^4} \tag{47}$$

which takes the following form:

$$P(x)\, y''(x) + Q(x)\, y'(x) + R(x)\, y(x) = S(x) \tag{48}$$

where,

$$P(x) = 1+2\eta D, \quad Q(x) = 2D - \frac{\theta'}{\theta-\theta_r}(1+2\eta D) - \frac{\theta-\theta_r}{\theta_r}(1-\varphi)^{2.5}\left(1-\varphi+\varphi\frac{\rho_S}{\rho_f}\right) f,$$
$$R(x) = \frac{\theta-\theta_r}{\theta_r}(1-\varphi)^{2.5}\left[1+\frac{3\left(\frac{\sigma_S}{\sigma_f}-1\right)\varphi}{\left(\frac{\sigma_S}{\sigma_f}+1\right)-\left(\frac{\sigma_S}{\sigma_f}-1\right)\varphi}\right] M + \frac{\theta-\theta_r}{\theta_r}(1-\varphi)^{2.5}\left(1-\varphi+\varphi\frac{\rho_S}{\rho_f}\right) f' \tag{49}$$
$$S(x) = \frac{\theta-\theta_r}{\theta_r}(1-\varphi)^{2.5}\frac{2\beta\theta}{(\eta+\alpha)^4}$$

Now Eq. (48) can be solved using a common finite difference method with central differencing and tridiagonal matrix manipulation. For that, the 2nd order ODEs of (48) can be written in the following way at the domain point x_n

$$P(x_n)\, y''(x_n) + Q(x_n)\, y'(x_n) + R(x_n)\, y(x_n) = S(x_n) \tag{50}$$

Using central differencing expansion, Eq. (49) may be expressed for y' term as

$$P(x_n)\frac{y_{n+1} - 2y_n + y_{n-1}}{\Delta x^2} + Q(x_n)\frac{y_{n+1} - y_{n-1}}{2\Delta x} + R(x_n)\, y_n = S(x_n) + O\left(\Delta x^2\right) \tag{51}$$

and this takes the form,

$$\left[\frac{P(x_n)}{\Delta x^2} - \frac{Q(x_n)}{2\Delta x}\right] y_{n-1} + \left[\frac{-2P(x_n)}{\Delta x^2} + R(x_n)\right] y_n + \left[\frac{P(x_n)}{\Delta x^2} + \frac{Q(x_n)}{2\Delta x}\right] y_{n+1} = S(x_n) + O\left(\Delta x^2\right) \tag{52}$$

To solve Eqs. (51) or (52), we drop the truncation error term $O\left(\Delta x^2\right)$ and of course there are namely N equations for one of each node. Thus the required N equations simultaneously written in one equation for each node as

$$\mathbf{Ay} = \mathbf{b} \tag{53}$$

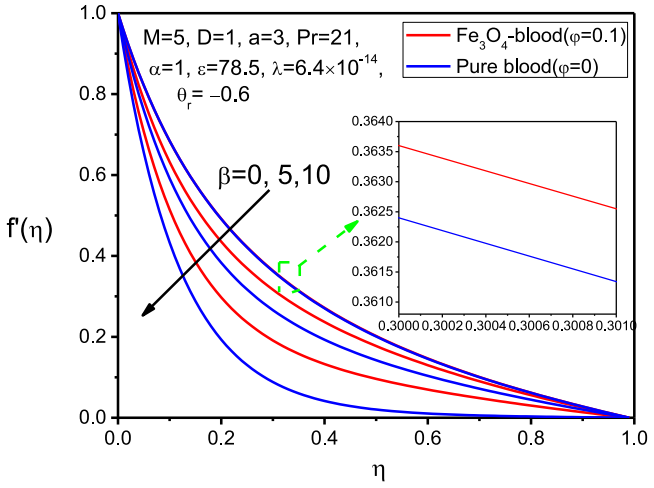

Fig. 2. Variations of $f'(\eta)$ with different values of β and φ.

Here, **A** is square matrix of size $N \times N$, thus the three non-zero diagonal are written along a row as

$$\begin{aligned} a_{n,n-1} &= \left[\frac{P(x_n)}{\Delta x^2} - \frac{Q(x_n)}{2\Delta x}\right] \\ a_{n,n} &= \left[\frac{-2P(x_n)}{\Delta x^2} + R(x_n)\right] \\ a_{n,n+1} &= \left[\frac{P(x_n)}{\Delta x^2} + \frac{Q(x_n)}{2\Delta x}\right] \end{aligned} \tag{54}$$

where the other entries a_{ij} become zero.

Since there are N node points, vector **b** can be written as

$$\mathbf{b} = \{S_1, S_2, S_3, \ldots\ldots\ldots, S_{n-1}, S_n, S_{n+1}, \ldots\ldots S_{N-1}, S_N\}^T \tag{55}$$

Where $S_n = S(x_n)$ and the unknown vector **y** as

$$\mathbf{y} = \{y_1, y_2, y_3, \ldots\ldots\ldots, y_{n-1}, y_n, y_{n+1}, \ldots\ldots, y_{N-1}, y_N\}^T \tag{56}$$

Now the required tridiagonal matrix form of Eq. (48) can be written as for $N = 5$,

$$\begin{bmatrix} a_{11} & a_{12} & 0 & 0 & 0 \\ a_{21} & a_{22} & a_{23} & 0 & 0 \\ 0 & a_{32} & a_{33} & a_{34} & 0 \\ 0 & 0 & a_{43} & a_{44} & a_{45} \\ 0 & 0 & 0 & a_{54} & a_{55} \end{bmatrix} \begin{bmatrix} y_1 \\ y_2 \\ y_3 \\ y_4 \\ y_5 \end{bmatrix} = \begin{bmatrix} b_1 \\ b_2 \\ b_3 \\ b_4 \\ b_5 \end{bmatrix} \tag{57}$$

According to [21], before starting the numerical procedure we need to assume the initial guesses for $f'(\eta)$ and $\theta(\eta)$ between $\eta = 0$ and $\eta = \eta_\infty$ $(\eta \to \infty)$ which satisfy the boundary conditions (22) and (23). For this, it is assumed as initial distributions that,

$$f'(\eta) = 1 - \frac{\eta}{\eta_\infty} \text{ and } \theta = 1 - \frac{\eta}{\eta_\infty}$$

These selected curves satisfy the boundary conditions. By integrating $f'(\eta)$ the distribution of $f(\eta)$ is derived. $\theta(\eta)$ is then retained, whereas the momentum Eq. (48) is solved using an algorithm employing a tridiagonal scheme, enabling a new approximation for $f'(\eta)$ to be produced. The distribution of $f(\eta)$ is updated by integrating the new estimation of $f'(\eta)$. These new profiles of $f'(\eta)$ and $f(\eta)$ are then used for new inputs, etc. Therefore, the momentum Eq. (48) is solved iteratively until the convergence is attained. The criterion of convergence involves

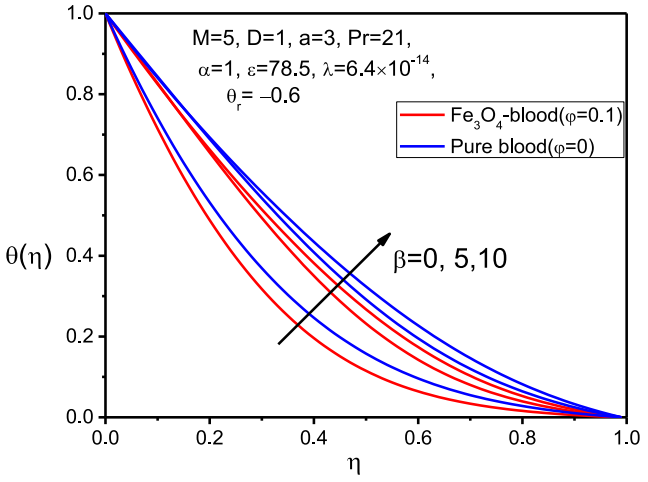

Fig. 3. Variations of $\theta\ (\eta)$ with different values of β and φ.

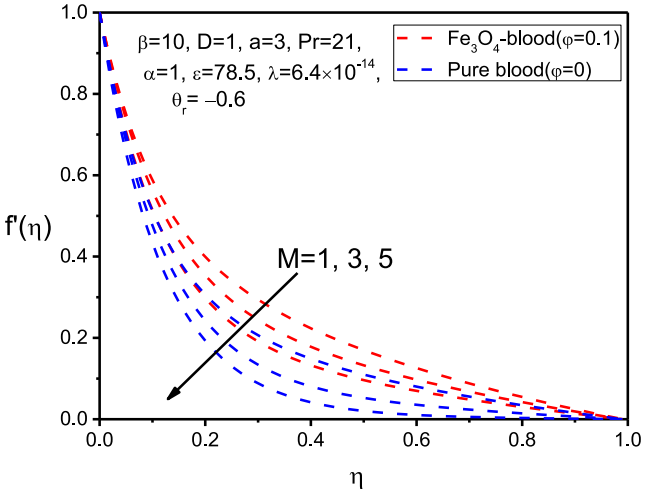

Fig. 4. Variations of $f'(\eta)$ with different values of M and φ.

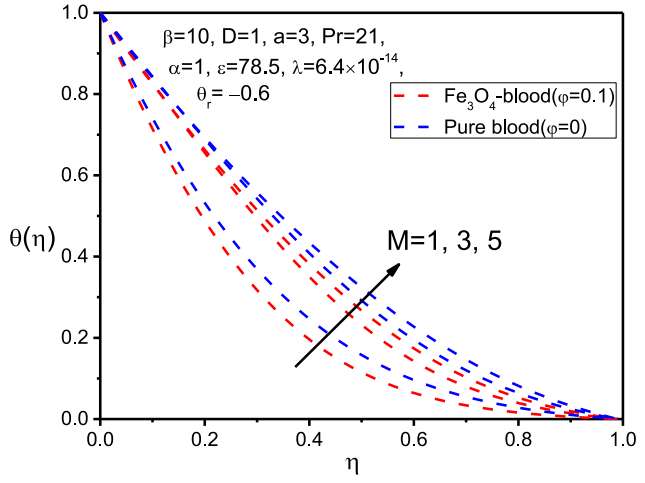

Fig. 5. Variations of $\theta\ (\eta)$ with different values of M and φ.

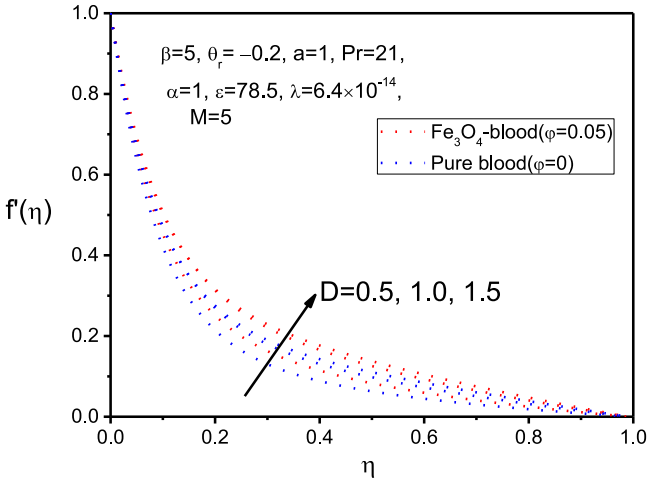

Fig. 6. Variations of $f'(\eta)$ with different values of D and φ.

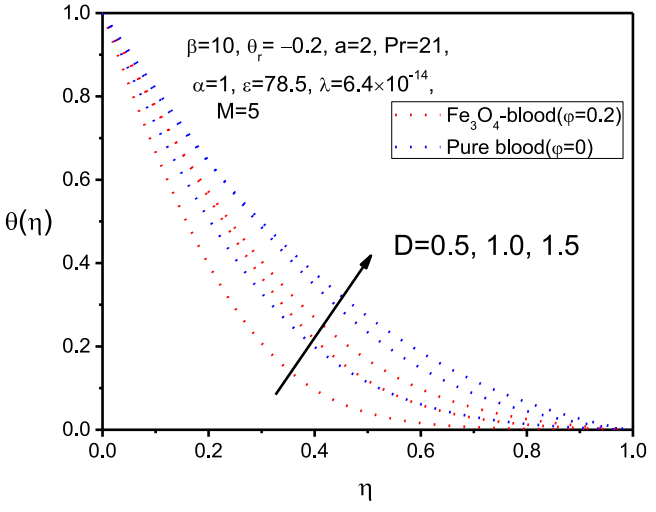

Fig. 7. Variations of $\theta(\eta)$ with different values of D and φ.

the values of the physically important gradient $f''(0)$ and the iterations stop when the difference in the values of $f''(0)$ between two successive iterations are less than a small quantity ε.

After $f'(\eta)$ is obtained, we solve the energy Eq. (21) with boundary conditions (22) and (23) using the same algorithm, but without iterations now, as the energy Eq. (21) is linear and it can be expressed as:

$$(1+a\theta)\,(1+2\eta D)\,\theta'' + \left[2\mathrm{D}\,(1+a\theta) + (1+2\eta D)\,a\,\theta' + \frac{\kappa_f}{\kappa_{mf}}\left(1-\varphi+\varphi\frac{(\rho C_P)_S}{(\rho C_P)_f}\right)\mathrm{Pr}\;\; f\right]\theta' + \frac{\kappa_f}{\kappa_{mf}}\frac{2\beta\lambda f}{(\eta+\alpha)^3}\theta = \frac{\kappa_f}{\kappa_{mf}}\frac{2\beta\lambda f\varepsilon}{(\eta+\alpha)^3} \tag{58}$$

By setting $y(x) = \theta(\eta)$, equation (4 50) is expressed in second-order linear differential equation form in the following way:

$$\mathbf{P}\,(\mathbf{x})\,\mathbf{y}''(\mathbf{x}) + \mathbf{Q}\,(\mathbf{x})\,\mathbf{y}'(\mathbf{x}) + \mathbf{R}\,(\mathbf{x})\,\mathbf{y}\,(\mathbf{x}) = \mathbf{S}\,(\mathbf{x}) \tag{59}$$

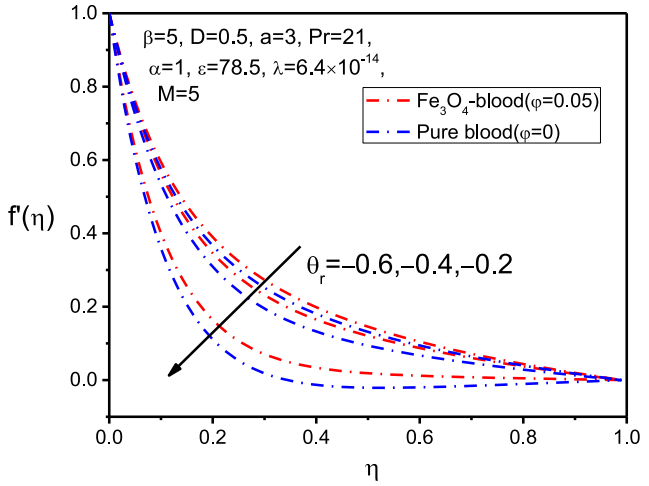

Fig. 8. Variations of $f'(\eta)$ with different values of θ_r and φ.

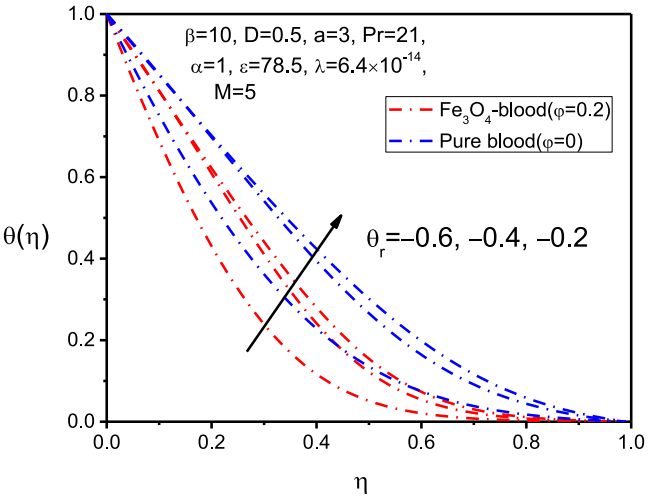

Fig. 9. Variations of $\theta\ (\eta)$ with different values of θ_r and φ.

where,

$$
\begin{aligned}
P\ (x) &= (1+a\theta)\ (1+2\eta D)\ ,\\
Q\ (x) &= \ 2\mathrm{D}\ (1+a\theta)+(1+2\eta D)\ a\,\theta' + \frac{\kappa_f}{\kappa_{mf}}\left(1-\varphi+\varphi\frac{(\rho C_P)_S}{(\rho C_P)_f}\right)\mathrm{Pr}\ \ f\ ,\\
R\ (x) &= \frac{\kappa_f}{\kappa_{mf}}\frac{2\beta\lambda f}{(\eta+\alpha)^3}\ ,\ \ S\ (x) = \frac{\kappa_f}{\kappa_{mf}}\frac{2\beta\lambda f\varepsilon}{(\eta+\alpha)^3}
\end{aligned}
\tag{60}
$$

In the whole numerical procedure, a step size of $h = \Delta\eta = 0.01$, $\eta_{\min} = 0$ and $\eta_{\max} = 1$ are applied and the solution is convergent with an approximation of 10^{-5}.

6. Numerical validation and thermophysical properties of magnetic particles ($Fe_3\ O_4$) and base fluid (blood)

To check the validity and accuracy of the numerical code, the present results are compared with those of Rangi et al. [36] for the skin friction coefficient when $M = 0$, $\beta = 0$, $\varphi = 0$, $\kappa_S = \kappa_f = 1$, which are shown in Table 1 and which were found to be in good agreement. Furthermore, in Table 2 the physical properties of blood and Fe_3O_4 are shown derived from earlier studies [4,23]. Finally, to obtain the grid suitable for the present mathematical model,

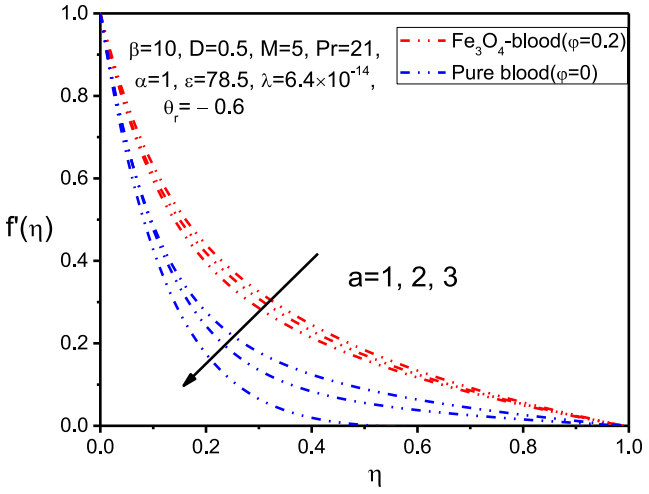

Fig. 10. Variations of $f'(\eta)$ with different values of a and φ.

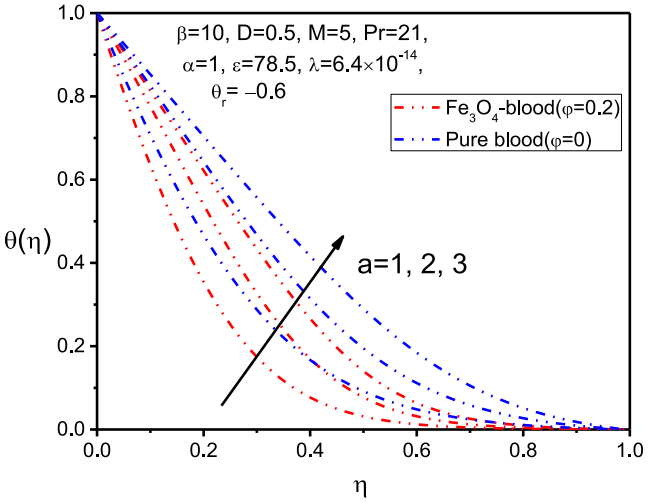

Fig. 11. Variations of $\theta(\eta)$ with different values of a and φ.

a grid independence test is studied here for ferromagnetic interaction parameter ($\beta = 0$, $\beta = 5$) and the obtained results are listed in Table 3. From Table 3, it is clearly seen that $\Delta\eta = 0.01$ grid provides an acceptable accurate results for the whole ranges of the BFD flows considered here.

7. Results and discussion

To obtain realistic results, previous studies related to the present formulation were taken into account in order to initiate a physically plausible case scenario of flow of blood as a base fluid. Thus, human body temperature is considered to be $T_w = 3°C$ [45] and body Curie temperature $T_c = 41°C$. For the above values it is obtained that the dimensionless temperature $\varepsilon = 78.5$ [30], viscous dissipation number $\lambda = 6.4 \times 10^{-14}$ [30] and dimensionless distance $\alpha = 1$ [18]. Moreover, the values of the leading parameters were as follows—the Prandtl number $\mathrm{Pr} = 21, 23, 25$ [18], magnetic field parameter $M = 1, 3, 5$ [4,30], volume fraction $\varphi = 0.0, 0.05, 0.1, 0.2$ [4], curvature parameter $D = 0.5, 1.0, 1.5$ [39], fluid viscosity variation parameter $\theta_r = -0.6, -0.4, -0.2$ [3], thermal

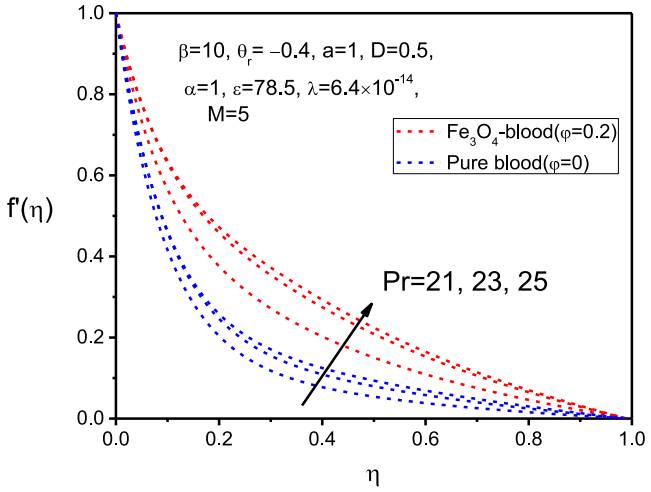

Fig. 12. Variations of $f'(\eta)$ with different values of Pr and φ.

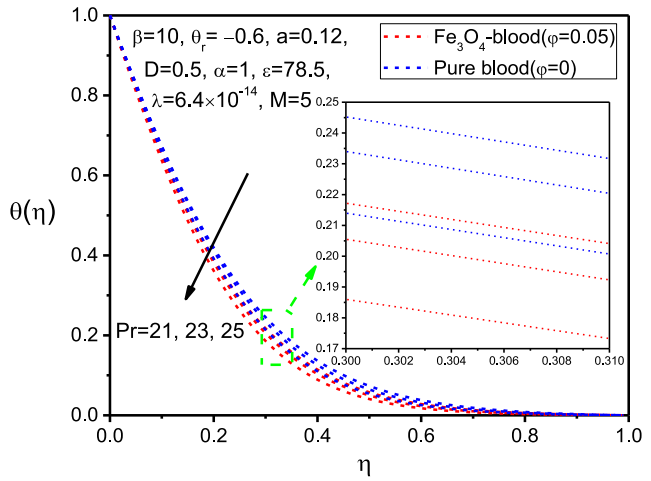

Fig. 13. Variations of $\theta(\eta)$ with different values of Pr and φ.

Table 1
Comparison of the skin friction coefficient ($f''(0)$) for various values of the curvature parameter D when $M = 0$, $\beta = 0$, $\varphi = 0$, $\kappa_S = \kappa_f = 1$.

D	Present results	Rangi et al. [36]
0.0	−1.005	−1.000
0.25	−1.006	−1.094378
0.5	−1.182	−1.188715
0.75	−1.283	−1.281833
1.0	−1.434	−1.459308

conductivity parameter $a = 1, 2, 3$ [34] and ferromagnetic interaction parameter $\beta = 0, 5, 10$ [4,30]. Note that $\phi = 0$ indicates pure blood flow and $\phi \neq 0$ indicates blood flow with magnetic particles.

Figs. 2 and 3 reveal the effects of the ferromagnetic interaction parameter on the axial velocity and temperature distributions in the presence of the magnetic particle volume fraction. Blood flow with magnetic particles (Fe_3O_4) is indicated in red, and the blue line shows the behavior of pure blood, meaning that no magnetic particles were

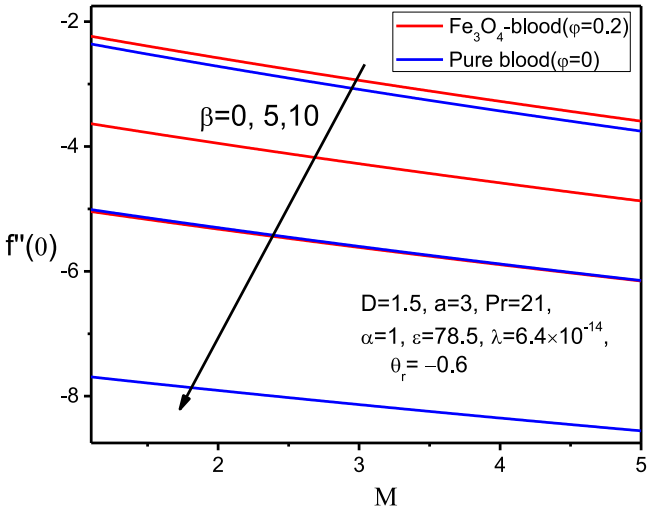

Fig. 14. Variation of $f''(0)$ with M for various values of β and φ.

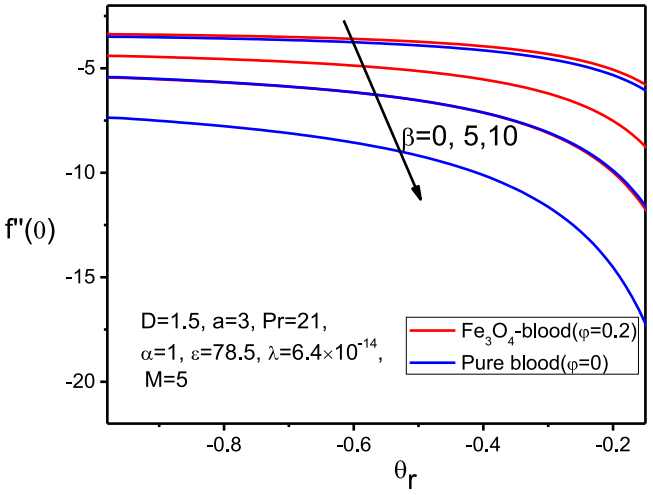

Fig. 15. Variation of $f''(0)$ with θ_r for various values of β and φ.

Table 2
Thermo-physical values of blood and Fe_3O_4.

Physical properties	C_p (J kg^{-1} K^{-1})	ρ (kg m^{-3})	σ (s m^{-1})	κ (W m^{-1} K^{-1})
Blood	3.9×10^3	1050	0.8	0.5
Fe_3O_4	670	5180	0.74×10^6	9.7

added. It is observed that blood-Fe_3O_4 velocity is decreased with rising values of the ferromagnetic number, and it is noticed that when magnetic particles were added into blood, its flow was much better compared to that of pure blood. However, in terms of the temperature profile, for pure blood is significantly increased, as can be seen in Fig. 3, compared to that with blood-Fe_3O_4. This occurs because of the relation between the Kelvin force and the ferromagnetic interaction parameter. This Kelvin force is also known as drug force. Such Kelvin force acts along fluid flow direction as a resistance force and thus, this results to reduction of the fluid velocity as well as

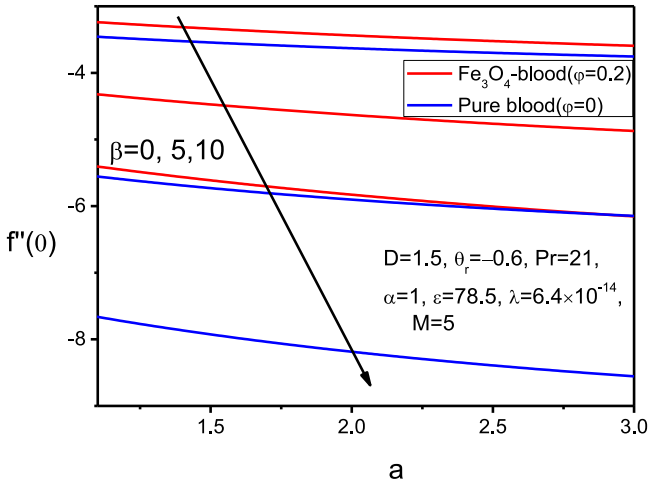

Fig. 16. Variation of $f''(0)$ with a for various values of β and φ.

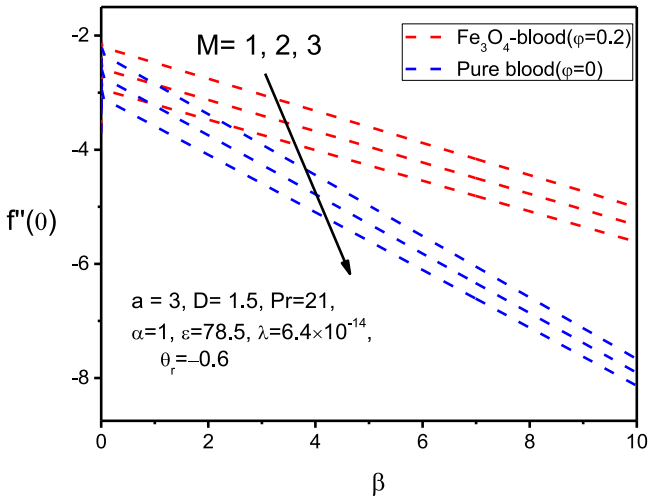

Fig. 17. Variation of $f''(0)$ with β for various values of M and φ.

Table 3
Grid independence test for $\beta = 0$ and $\beta = 5$ while other parameter values are $\alpha = 1, \varepsilon = 78.5, \mathrm{Pr} = 21, a = 3, D = 1, M = 5, \lambda_1 = 6.4 \times 10^{-14}, \theta_r = -0.1, \phi = 0.2$.

Step size $h = \Delta\eta$	η	$\beta = 0$		$\beta = 5$		CPU time
		f'	θ	f'	θ	
0.01	0.04	0.7471	0.8716	0.6622	0.9274	1.248 s
	0.08	0.5758	0.7539	0.4443	0.854	
0.02	0.04	0.7474	0.8715	0.663	0.9274	0.842 s
	0.08	0.5761	0.7537	0.4455	0.8539	
0.04	0.04	0.7487	0.8712	0.6661	0.9273	0.655 s
	0.08	0.5778	0.753	0.4499	0.8536	

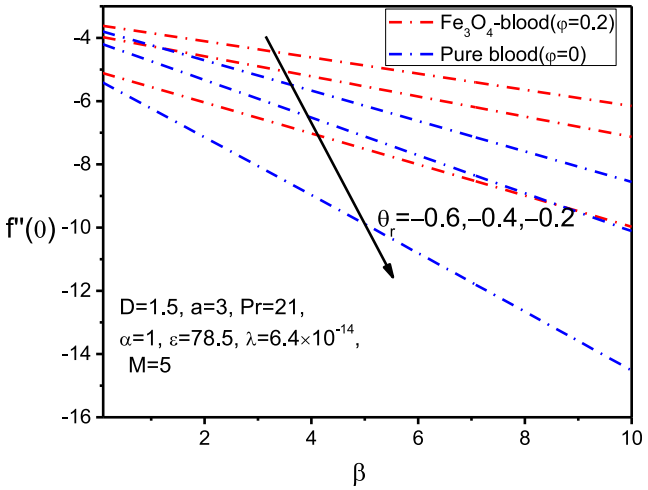

Fig. 18. Variation of $f''(0)$ with β for various values of θ_r and φ.

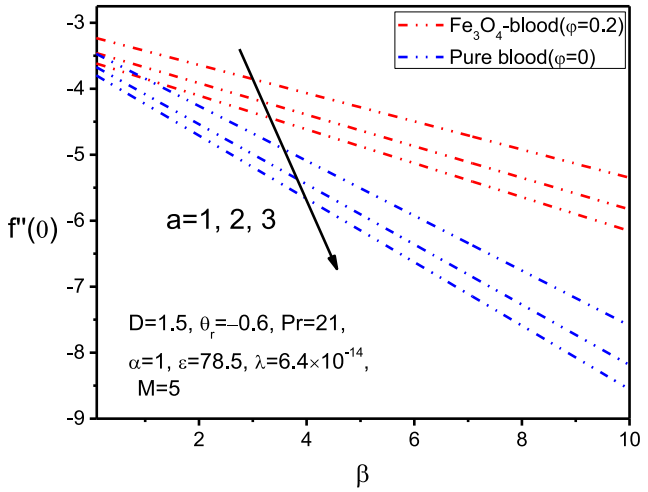

Fig. 19. Variation of $f''(0)$ with β for various values of a and φ.

temperature enhancement. From these figures, it is also evident that blood flow can be significantly influenced by the presence of ferromagnetic number.

The effects of the magnetic field parameter, along with magnetic particle volume fraction, are shown in Figs. 4 and 5. Since the magnetic field produces a Lorentz force that acts in the direction reverse of the flow. As a result, when the values of Lorentz force are gradually increased, the fluid velocity decreases. The opposite behavior of the temperature is observed where the temperature profile is enhanced with the increment of the Lorentz force. This is clearly apparent in Figs. 4 and 5. Furthermore, it is also evident from these figures that the velocity of the fluid with magnetic particles, i.e., blood-Fe_3O_4, is slightly enhanced compared to that of pure blood, and vice versa for the temperature profile.

The variation effects of the magnetic particle volume fraction on velocity and temperature profiles, along with the impact of the curvature parameter, are presented at Figs. 6 and 7. Interestingly, from Figs. 6 and 7 it is noticed that both velocity and temperature distributions were enhanced with accretive values of the curvature parameter. It is well known that when the values of the curvature parameter are enhanced, the cylinder's radius comes down, as a result the surface area is reduced, causing less resistance to the blood's motion. Consequently, the blood flow

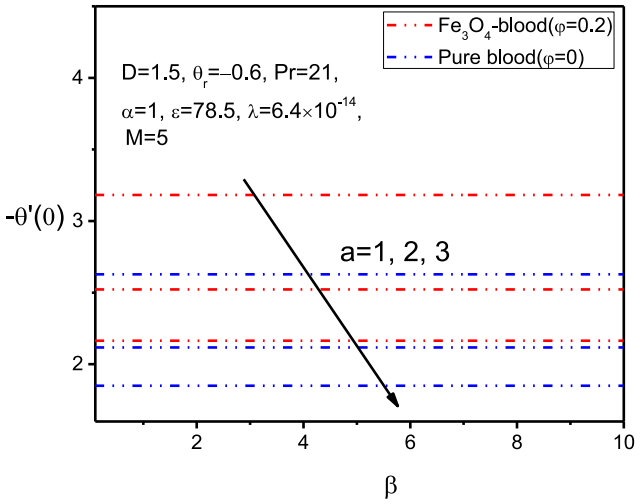

Fig. 20. Variation of $-\theta'(0)$ with β for various values of a and φ.

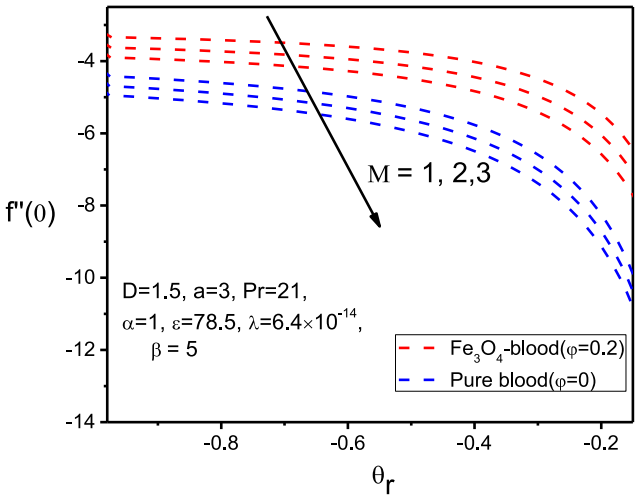

Fig. 21. Variation of $f''(0)$ with θ_r for various values of M and φ.

accelerates and this can be observed from the plotted figures. However, the heat transfer of fluid becomes faster form surface to blood when the values of curvature parameter are one or above.

Figs. 8 and 9 demonstrate the characteristics of the viscosity variation parameter, along with the magnetic particle volume fraction, on the velocity and temperature profiles. As the viscosity variation parameter increases, the velocity profile decreases but the temperature profile is enhanced. This is because when the values of θ_r are getting higher, the velocity thickness of the boundary layer in the horizontal direction is decreased. Physically, higher values of θ_r express the difference in temperature between the ambient fluid and the cylindrical surface and it causes to augmentation of the temperature distribution.

Figs. 10 and 11 show the influence of the thermal conductivity parameter on velocity and temperature distributions when $\varphi = 0.2$ and $\varphi = 0.0$. These two figures reveal that when the values of thermal conductivity parameter are gradually increased, the fluid velocity profile decreases, whereas the opposite occurs for the temperature profile. Due to the fact that the enhancement of the values of the temperature-dependent thermal conductivity parameter results to increase the thermal conductivity of electrically conducting fluids such as blood. Consequently, the heat of the fluid is rapidly transferred through the blood (human body), since the thermal conductivity of the material is much higher.

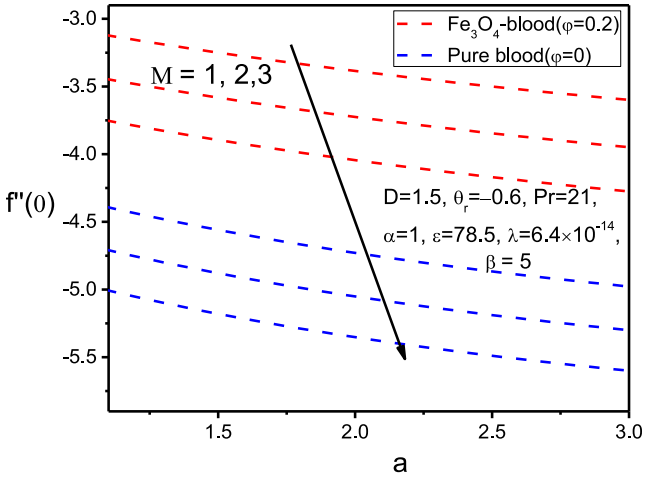

Fig. 22. Variation of $f''(0)$ with a for various values of M and φ.

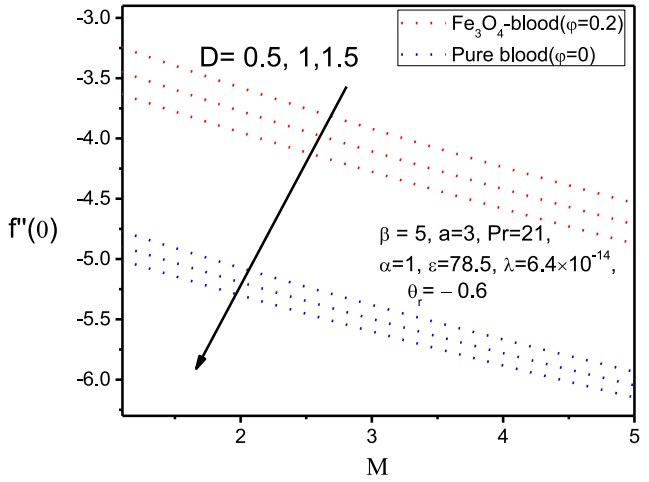

Fig. 23. Variation of $f''(0)$ with M for various values of D and φ.

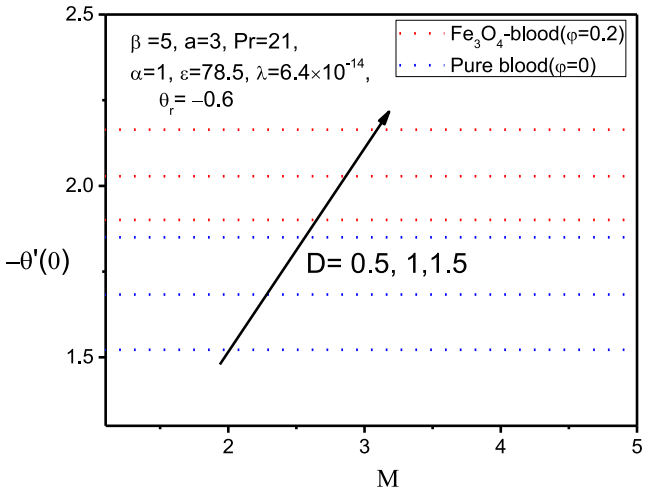

Fig. 24. Variation of $-\theta'(0)$ with M for various values of D and φ.

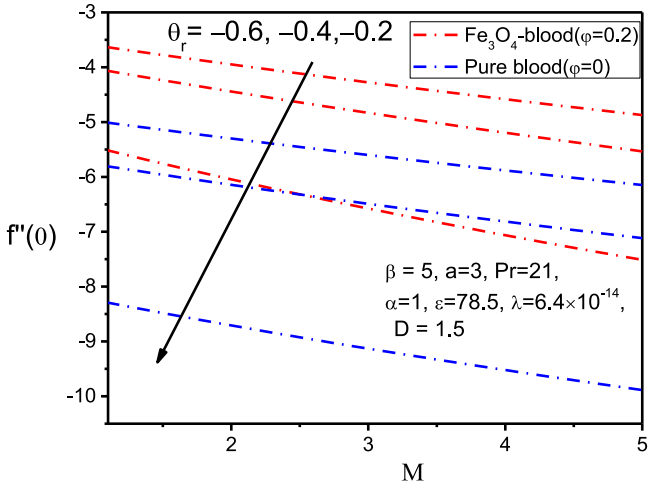

Fig. 25. Variation of $f''(0)$ with M for various values of θ_r and φ.

The effects of the Prandtl number on velocity and temperature profiles in the presence of the magnetic particle volume fraction are demonstrated in Figs. 12 and 13. It was obviously expected that the velocity profile is increased as the values of Prandtl number increased, and the temperature profile is decreased. These outcomes are clearly seen in Figs. 12 and 13. This is justified from the fact that the Prandtl number is the ratio between momentum diffusivity and thermal diffusivity. Thus, higher values of the Prandtl number indicate that the momentum of fluid velocity is increased in the boundary layer.

Finally, the variations of the skin friction coefficient and the rate of heat transfer, in terms of parameters such as the ferromagnetic interaction parameter, magnetic field parameter, viscosity variation parameter, and thermal conductivity parameter, are demonstrated in Figs. 14 to 27. Figs. 14 to 16 show the influence of the ferromagnetic number with the magnetic volume fraction on the skin friction coefficient with regard to the magnetic field parameter, the viscosity variation parameter and the thermal conductivity parameter, respectively. In all those cases, the skin friction coefficient was decreased, and it was found that when magnetic particles were added to the base fluid (blood), values were slightly enhanced compared to that of pure blood.

Figs. 17 to 20 display the impact of the magnetic parameter, the viscosity variation parameter and the thermal conductivity parameter in the presence of the magnetic particle volume fraction on the skin friction coefficient and the rate of heat transfer with regard to the ferromagnetic interaction parameter. It is clearly evident in the figures that skin friction decreases, and the rate of heat transfer (only for the thermal conductivity parameter) is also reduced as the values of these parameters is increased. Furthermore, Figs. 21 and 22 illustrate the influence of the magnetic field parameter on the skin friction coefficient with regard to the viscosity variation parameter and the thermal conductivity parameter, showing the same results.

The variations of the skin friction coefficient and the rate of heat transfer under the influence of the curvature parameter, the viscosity variation parameter, and the thermal conductivity parameter with the magnetic particle volume fraction with regard to the magnetic field parameter are demonstrated in Figs. 23 to 27. For the curvature parameter, the skin friction coefficient is reduced, whereas rate of heat transfer increases in this case. However, both skin friction coefficient and rate of heat transfer are decreased with the increment in the thermal conductivity parameter, whereas the skin friction coefficient decreases for the viscosity variation parameter.

8. Concluding remarks

An application of the mathematical model of BFD is carried out for the study of blood flow with magnetic particles over a two-dimensional stretching cylinder. This model involves both MHD and FHD principles. In addition, the effects of temperature dependent variables of fluid viscosity and thermal conductivity were considered. Moreover, blood flow in two separated cases is also investigated namely pure blood and blood with magnetic particles. Using a similarity transformation, the governing partial differential equations were converted into ordinary

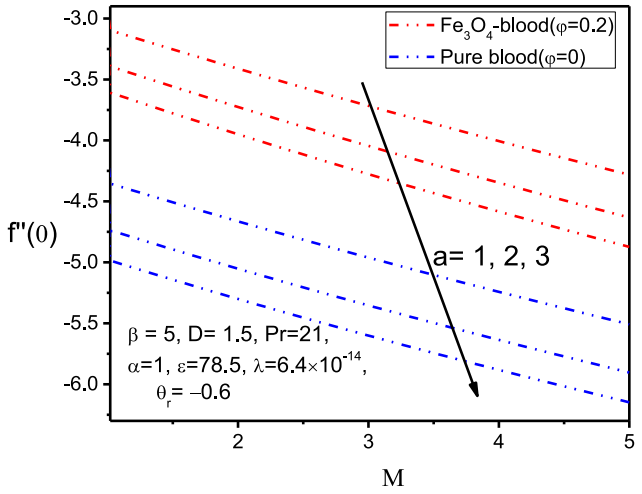

Fig. 26. Variation of $f''(0)$ with M for various values of a and φ.

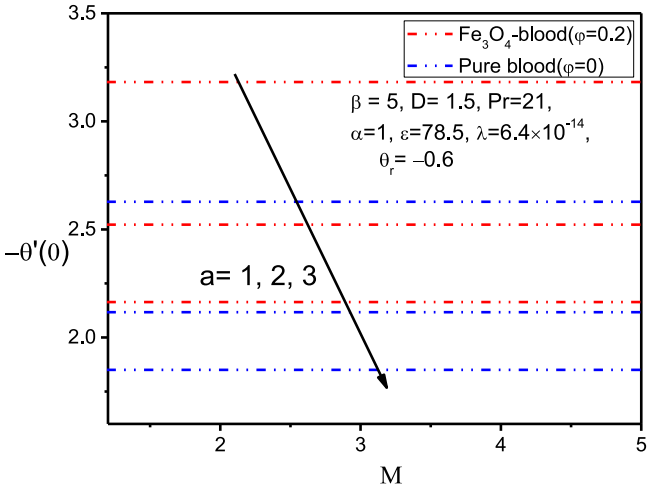

Fig. 27. Variation of $-\theta'(0)$ with M for various values of a and φ.

differential equations along with the corresponding boundary conditions. A temporal stability analysis was also carried out and the numerical results were obtained using an efficient technique based on a common finite difference method with central differencing, tridiagonal matrix manipulation and an iterative procedure. The hope is that the present analysis will be utilized in the biomedicine and bioengineering sectors especially in targeted molecule, MRI, cancer therapy etc. The proposed mathematical model shows that under certain conditions blood flow can be controlled by employing a strong magnetic field in boundary layer region, and where magnetic particles play an emergent role. The main points derived from the present analysis are listed below:

- A rise in ferromagnetic interaction parameter, the magnetic field parameter, the viscosity variation parameter, and the thermal conductivity parameter, causes decrement of the fluid velocity, whereas the temperature profile was enhanced in all these cases. It is noted that the velocity of the blood-Fe_3O_4 mixture was significantly increased compared to the fluid velocity of pure blood, and the opposite trend was found in the temperature distribution.
- Both velocity and temperature distributions were enhanced when the values of the curvature parameter was gradually increased.

- When the Prandtl number is enhanced, the velocity distribution is increased, whereas the temperature profile is decreased.
- Increment of the ferromagnetic interaction parameter, the magnetic field parameter and the viscosity variation parameter yields the skin friction coefficient to decline.
- The curvature parameter tends to decrease the skin friction coefficient but enhance the rate of heat transfer.
- Both skin friction coefficient and rate of heat transfer are increased when the values of thermal conductivity are increased.

The proposed mathematical formulation may be expanded for other indispensable subclasses of non-Newtonian fluid such as Powell–Eyring fluid, Maxwell fluid and many others. Additionally, the effects of thermal radiation may be discussed for the present model in future along with boundary slip conditions. Moreover, the effects of magnetic/non-magnetic particles shape factor could also be investigated in future. It is hoped that the proposed BFD modeling will further be validated using new experimental data.

References

[1] W. Abbas, A.M. Megahed, Powell-Eyring fluid flow over a stratified sheet through porous medium with thermal radiation and viscous dissipation, AIMS Math. 6 (12) (2021) 13464–13479.
[2] H. Abdi, S.Y. Motlagh, H. Soltanipour, Study of magnetic nanofluid flow in a cavity under the magnetic field of a wire carrying the electric current in turbulence regime, Results Phys. 18 (2020) 103224.
[3] M.J. Alam, M.G. Murtaza, Effect of temperature dependent viscosity on biomagnetic fluid flow and heat transfer over a nonlinear stretching sheet, J. Adv. Technol. Eng. Res. 6 (1) (2020) 08–21, http://dx.doi.org/10.20474/jater-6.1.2.
[4] J. Alam, G. Murtaza, E. Tzirtzilakis, M. Ferdows, Biomagnetic fluid flow and heat transfer study of blood with gold nanoparticles over a stretching sheet in presence of magnetic dipole, Fluids 6 (113) (2021).
[5] M.J. Alam, M.G. Murtaza, E.E. Tzirtzilakis, M. Ferdows, Effect of thermal radiation on biomagnetic fluid flow and heat transfer over an unsteady stretching sheet, Comput. Assist. Methods Eng. Sci. (CAMES) 28 (2) (2021) 81–104, http://dx.doi.org/10.24423/cames.327.
[6] F. Ali, S. Majeed, A. Imtiaz, Magnetohydrodynamic blood flow in a cylindrical tube with magnetic particles: A time fractional model, Math. Probl. Eng. (2021) 6624912, http://dx.doi.org/10.1155/2021/6624912.
[7] M. Amer Qureshi, Numerical simulation of heat transfer flow subject to MHD of Williamson nanofluid with thermal radiation, Symmetry 13 (10) (2021) http://dx.doi.org/10.3390/sym13010010.
[8] M.K. Anuar Mohamed, F.N. Abas, M.Z. Salleh, MHD boundary layer flow over a permeable flat plate in a ferrofluid with thermal radiation effect, J. Phys. Conf. Ser. 1366 (2019) 012014, http://dx.doi.org/10.1088/1742-6596/1366/1/012014.
[9] S.U.S. Choi, Enhancing thermal conductivity of fluids with nanoparticles, in: Proceedings of the ASME International Mechanical Engineering Congress and Exposition San Francisco, CA, USA, vol. 9, 1995, pp. 9–105.
[10] B. Dubertret, P. Skourides, D.J. Norris, V. Noireaux, A.H. Brivanlou, In vivo imaging of quantum dots encapsulated in phospholipids micelles, Science 298 (5599) (2002) 1759–1762.
[11] S. Durr, C. Janko, S. Lyer, P. Tripal, M. Schwarz, J. Zaloga, R. Toetze, C. Alexiou, Magnetic nanoparticles for cancer therapy, Nanotechnol. Rev. 2 (4) (2013) 395–409.
[12] M. Ferdows, M.G. Murtaza, E.E. Tzirtzilakis, F. Alzahrani, Numerical study of blood flow and heat transfer through stretching cylinder in the presence of a magnetic dipole, Zeitschrift Fur Angewandte Mathematik Und Mechanik (2020) e201900278, http://dx.doi.org/10.1002/zamm.201900278.
[13] M. Ferdows, M.G. Murtaza, E.E. Tzirtzilakis, J.C. Misra, F. Alzahrani, Dual solutions for boundary layer flow and heat transfer of biomagnetic fluid over a stretching/shrinking sheet in presence of a magnetic dipole and prescribed heat flux, Int. J. Appl. Electromagn. Mech. 65 (2021) 235–251.
[14] J.A. Gbadeyan, E.O. Titilloye, A.T. Adeosun, Effects of variable thermal conductivity and viscosity on casson nanofluid flow with convective heating and velocity slip, Heliyon 6 (2020) e03076.
[15] S. Goodwin, Magnetic targeted carries offer site-specific drug delivery, Oncol. News Int. 9 (22) (2000).
[16] Y. Haik, J.C. Chen, V.M. Pai, Development of bio-magnetic fluid dynamics, in: S.H. Winoto, Y.T. Chew, N.E. Wijeysundera (Eds.), Proceedings of the IX International Symposium on Transport Properties in Thermal Fluids Engineering, Singapore, Pacific Center of Thermal Fluid Engineering, Hawaii, USA, 1996, pp. 121–126.
[17] S.D. Harris, D.B. Ingham, I. Pop, Mixed convection boundary layer flow near the stagnation point on a vertical surface in a porous medium: Brinkman model with slip, Trans. Porous Media 77 (2) (2009) 267–285.
[18] S. Hazarika, S. Ahmed, Theoretical investigation of viscosity and thermal conductivity of a Gas along a non-isothermal vertical surface in porous environment with dissipative heat: Numerical technique, J. Appl. Comput. Mech (2021) 1–10, http://dx.doi.org/10.22055/JACM.2021.35353.2638.
[19] S. Hazarika, S. Ahmed, A.J. Chakma, Analysis of platelet shape Al2O3 and TiO2 on heat generative hydromagnetic nanofluids for the base fluid C2H6O2 in a vertical channel of porous medium, Walailak J. Sci. Tech. 18 (14) (2021) 21424.
[20] Z. Hussain, Temperature dependent viscosity hybrid nanofluid subject to homogeneous-heterogeneous reactions and melting condition: A comparative study, Phys. Scr. 96 (1) (2020) 015210.
[21] N.G. Kafoussias, E.W. Williams, An improved approximation technique to obtain numerical solution of a class of two point boundary value similarity problems in fluid mechanics, Internat. J. Numer. Methods Fluids 17 (1993) 145–162.

[22] A. Karimipour, A. D'Orazio, M.S. Shadloo, The effects of different nanoparticles of Al2O3 and Ag on MHD nanofluid flow and heat transfer in a microchannel including slip velocity and temperature jump, Physica E 86 (2017) 146–153.
[23] K.A. Kumar, N. Sandeep, V. Sugunamma, I.L. Animasaun, Effect of irregular heat source/sink on the radiative thin film flow of MHD hybrid ferrofluid, J. Thermal Anal. Calorim. 139 (2020) 2145–2153.
[24] J. Lu, S. Ma, J. Sun, C. Xia, C. Liu, Z. Wang, Magnetese ferrite nanoparticle micellarnanocomposites as MRI contrast agent for liver imaging, Biomaterials 30 (2009) 2919–2928.
[25] O.D. Makinde, Stagnation point flow with heat and mass transfer and temporal stability of ferrofluid past a permeable stretching/shrinking sheet, Defect Diffusion Forum 387 (2018) 510–522.
[26] A.M. Megahed, Carreau fluid flow due to nonlinearly stretching sheet with thermal radiation, heat flux, and variable conductivity, Appl. Math. Mech. 40 (11) (2019) 1615–1624.
[27] A.M. Megahed, M.G. Reddy, W. Abbas, Modeling of MHD fluid flow over an unsteady stretching sheet with thermal radiation, variable fluid properties and heat flux, Math. Comput. Simulation 185 (2021) 583–593.
[28] A. Mishra, M. Kumar, Velocity and thermal slip effects on MHD nanofluid flow past a stretching cylinder with viscous dissipation and joule heating, SN Appl. Sci. 2 (2020) 1350, http://dx.doi.org/10.1007/s42452-020-3156-7.
[29] M.G. Murtaza, M. Ferdows, E.E. Tzirtzilakis, J.C. Misra, Three dimensional biomagnetic Maxwell fluid flow over a stretching surface in presence of heat source/sink, Int. J. Biomath. 12 (3) (2019) 12.
[30] M.G. Murtaza, E.E. Tzirtzilakis, M. Ferdows, Effect of electrical conductivity and magnetization on the biomagnetic fluid flow over a stretching sheet, Zeitschrift Fur AngewandteMathematik Und Physik 68 (93) (2017).
[31] M.G. Murtaza, E.E. Tzirtzilakis, M. Ferdows, Stability and convergence analysis of a biomagnetic fluid flow over a stretching sheet in the presence of a magnetic field, Symmetry 12 (253) (2020).
[32] S. Nadeem, N. Ullah, A.U. Khan, T. Akbar, Effect of homogeneous-heterogeneous reactions on ferrofluid in the presence of magnetic dipole along a stretching cylinder, Results Phys. 7 (2017) 3574–3582.
[33] C. Plank, F. Scherer, U. Schillinger, C. Bergemann, M. Anton, Magnetofection: Enhancing and targeting gene delivery with superparamagnetic nanoparticles and magnetic fields, J. Liposome Res. 13 (2003) 29–34.
[34] U. Rahid, D. Baleanu, H. Liang, M. Abbas, A. Iqbal, J. Ul-Rahman, Marangoni boundary layer flow and heat transfer of graphene-water nanofluid with particle shape effects, Processes 8 (1120) (2020) http://dx.doi.org/10.3390/pr8091120.
[35] C. Rajashekhar, G. Manjunatha, K.S. Basavarajappa, Analytical solution of FHD flow of blood through layered model in the presence of magnetic field, J. Mech. Eng. Res. Dev. 40 (2) (2017) 365–370.
[36] R.R. Rangi, N. Ahmad, Boundary layer flow past a stretching cylinder and heat transfer with variable thermal conductivity, Appl. Math. 3 (2012) 205–209.
[37] S.O. Salawu, M.S. Dada, The radiative heat transfer of variable viscosity and thermal conductivity effects on inclined magnetic field with dissipation in a non-Darcy medium, J. Nigerian Math. Soc. 35 (2016) 93–106.
[38] S. Siddiqs, S. Naqvi, N. Begum, A. Hossain, Thermal radiation therapy of biomagnetic fluid flow in the presence of localized magnetic field, Int. J. Therm. Sci. 132 (2018) 457–465, http://dx.doi.org/10.1016/j.ijthermalsci.2018.06.023.
[39] P. Sreenivasulu, T. Poornima, N.B. Reddy, Variable thermal conductivity influence on hydromagnetic flow past a stretching cylinder in a thermally stratified medium with heat source/sink, Front. Heat Mass Transf. (FHMT) 9 (20) (2017) http://dx.doi.org/10.5098/hmt.9.20.
[40] D.D. Stark, R. Weissleder, G. Elizondo, P.F. Hahn, S. Saini, L.E. Todd, J. Wittenberg, J.T. Ferucci, Superparamagnetic iron oxide: clinical application as a contrast for MR imaging of the liver, Radiology 168 (1988) 297–301.
[41] H. Tahir, U. Khan, A. Din, Y.U. Chu, N. Muhammad, Heat transfer in a ferromagnetic chemically reactive species, J. Thermo-Phys. Heat Transf. (2020) http://dx.doi.org/10.2514/1.T6143.
[42] E.E. Tzirtzilakis, A mathematical model for blood flow in magnetic field, Phys. Fluids 17 (7) (2005) 077103-077114.
[43] E.E. Tzirtzilakis, N.G. Kafoussias, Three dimensional magnetic fluid boundary layer flow over a linearly stretching sheet, J. Heat Transfer 132 (1) (2010) 1–8.
[44] E.E. Tzirtzilakis, G.B. Tanoudis, Numerical study of biomagnetic fluid flow over a stretching sheet with heat transfer, Internat. J. Numer. Methods Heat Fluid Flow 13 (7) (2003) 830–848.
[45] E.E. Tzirtzilakis, M. Xenos, V.C. Loukopoulos, N.G. Kafoussias, Turbulent biomagnetic fluid flow in a rectangular channel under the action of a localized magnetic field, Internat. J. Engrg. Sci. 44 (18–19) (2006) 1205–1224.
[46] P.D. Weidman, D.G. Kubitschek, A.M.J. Davis, The effects of transpiration on self-similar boundary layer flow over moving surfaces, Internat. J. Engrg. Sci. 44 (2006) 730–737.